Article

Polarimetric imaging VS conventional imaging: evaluation of image contrast in fog

Maria Ballesta-Garcia *, Sara Peña-Gutiérrez, Aina Val-Martí and Santiago Royo

Centre for Sensor, Instrumentation and Systems Development, Universitat Politècnica de Catalunya (CD6-UPC), Rambla Sant Nebridi 10, E08222 Terrassa, Spain.

* Correspondence: maria.ballesta.garcia@upc.edu.

Abstract: An evaluation of image contrast in a controlled foggy environment has been made by comparison between intensity imaging and different modes of polarimetric imaging. A small-scale fog chamber has been designed and constructed to create the necessary controlled foggy environment. A linear polarimetric camera of division of focal plane and a linearly polarized light source has been used for performing the experiments with polarized light. In order to evaluate the image contrast of the different imaging modes, the Michelson's contrast of samples of different materials relative to their background has been calculated. The higher the image contrast, the easier is to detect and segment the targets of interest that are surrounded by fog. It has been proved quantitatively that in the studied situations polarimetric images present an improvement in contrast when compared to conventional intensity images.

Keywords: turbid media; fog; polarimetry; memory effect; polarimetric imaging; image processing; contrast; detection.

1. Introduction

When light propagates through a turbid media, the direction of propagation is randomized faster than its initial state of polarization. As a consequence, light is attenuated before the initial polarimetric properties are lost. This effect is known as polarization memory effect [1-3]. The prolonged maintenance of the polarimetric state causes, in given conditions, that polarimetric images show better image contrast than conventional (intensity or RGB) images [4-6]. With higher contrast, distinguishing and detecting objects in the scene of interest is easier. For this reason, images obtained by detecting polarimetric properties are a suitable alternative for imaging in applications through turbid media [7]. Fields like navigation, transport or surveillance could take advantage of this phenomenon. For these applications, it is essential the detection and identification of targets through adverse weather conditions such as fog or smoke. Conventional imaging is often limited and breaks down at low visibilities. Due to the aforementioned characteristics, polarimetric imaging is being explored as a possible solution to surpass this limit [8-13].

Polarization can be described using different formalisms. Here, the Stokes vector $\vec{S}$ is used to characterize the polarization state of a light beam [14]. **S** is determined from to the six irradiance measurements of the light beam showed in Table 1.

Table 1. Irradiance measurements I (W/m^2) taken with ideal polarizers in front of a radiometer.

Name	Measurements
I_H	Horizontal linear polarizer (0 deg)
I_V	Vertical linear polarizer (90 deg)
I_{45}	45 deg linear polarizer
I_{135}	135 deg linear polarizer
I_L	Left circular polarizer
I_R	Right circular polarizer

Using the measurements presented in Table 1, the Stokes vector, specified relative to a local x—y coordinate system defined in the plane perpendicular to the propagation vector, is defined as:

$$\vec{\boldsymbol{S}} = \begin{pmatrix} I_H + I_V \\ I_H - I_V \\ I_{45} - I_{135} \\ I_R - I_L \end{pmatrix} = \begin{pmatrix} S_0 \\ S_1 \\ S_2 \\ S_3 \end{pmatrix}, \tag{1}$$

where S_0, S_1, S_2 and S_3 are the Stokes vector elements.

The polarized portion of the beam represents a net polarization ellipse traced by the electric field vector as a function of time. This ellipse has an ellipticity (ε) and an orientation of the major axis (η) (azimuth of the ellipse) measured counterclockwise from the x axis such that:

$$\varepsilon = \frac{S_3}{S_0 + \sqrt{S_1^2 + S_2^2}}, \tag{2}$$

$$\eta = \frac{1}{2}\arctan\left(\frac{S_2}{S_1}\right). \tag{3}$$

From $\vec{\boldsymbol{S}}$, characteristics of the light beam such as the total irradiance (I), the Degree of polarization (DOP) and the Degree of linear polarization (DOLP) can be directly derived as:

$$I = S_0, \tag{4}$$

$$DOP = \frac{\sqrt{S_1^2 + S_2^2 + S_3^2}}{S_0}, \tag{5}$$

$$DOLP = \frac{\sqrt{S_1^2 + S_2^2}}{S_0}. \tag{6}$$

In this article, we present a study of contrast of different modes of imaging in fog, comparing images obtained by means of intensity and polarization properties of light. Recently, due to the growth of potential applications of polarimetry in turbid media, these kinds of studies have become popular. Previous researchers have developed experiments using different types of targets and backgrounds, involving scattering, absorption and reflection targets. It has been shown that the contrast improvement depends on the optical properties regarding polarized light of the background and the target [15,16]. Outdoor testing in fog has also been done [17]. Another factor to take into account is the polarimetric response of fog. When interacting with fog, incident light experiences a sequence of near-forward-scattering events before it contributes to the backscattered light. As a result, the backscattering due to fog is depolarized with a detectable component in the same polarization of incidence [2].

Our study is based on inspecting different types of common materials with different polarimetric properties and colors (paper, wood, plastic and metal), submerged in a media that reassembles actual fog. In order to perform these experiments, we have developed an experimental setup capable of producing, containing and control a foggy medium with the desired characteristics. Its construction and characteristics are detailed in next section.

2. Materials and Methods

2.1. Experimental setup

2.1.1. Fog chamber

The experiment was carried out by developing and constructing a small-scale fog chamber enabling to reproduce, characterize and control different levels of fog visibility. Its schematics may be found in Fig. 1(a) and the real photograph in Fig. 1(b).

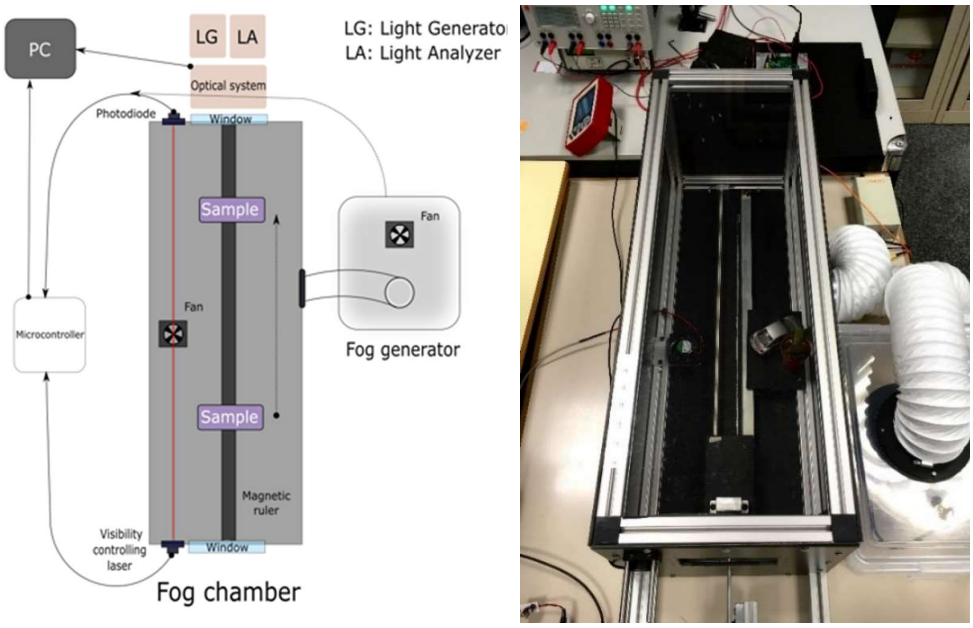

(a) **(b)**

Figure 1. Small-scale fog chamber. Experimental setup used to perform the experiments: (**a**) Schematics; (**b**) Image of the fog chamber.

The fog chamber consisted of a 300x300x900 mm box with an aluminum structure covered by black methacrylate panels. The fog was generated in an external container and was injected into the box through a 10 cm diameter hole at its side using a fan. Due to its characteristics, the fog entering the chamber tended to accumulate in layers at the bottom. An additional fan inside the box was used to uniformly distribute the accumulated fog which was layering within the box. One of the squared ends of the box had a hole in which the illumination and the detection optical systems were placed in the same geometrical plane. In the upper part of the chamber, an additional longitudinal optical path was enabled with a photodiode aligned to a collimated laser light at 635 nm. These two elements were used to calibrate at all times the level of fog in the chamber through the experimentally measured optical transmittance (T):

$$T = I/I_0, \tag{7}$$

where I is the optical power measured at each moment and I_0 is the initial optical power, when there is no fog in the box. Fig. 2 shows the evolution of a typical cycle of dissipation of fog inside the box as a function of time.

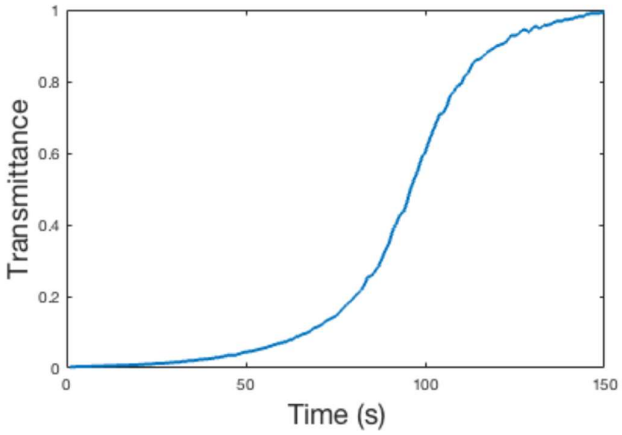

Figure 2. Typical cycle of fog dissipation inside the fog chamber. Plot shows Transmittance versus Time.

2.1.2. Illumination

In order to perform the experiments, a white light source model SCHOTT KL 1500 ELECTRONIC with linear polarizer duly aligned was used. The polarization state of light was calibrated with a polarimeter model PAX1000VIS/M from THORLABS. The light was almost perfectly linearly polarized at 0 deg relative to the horizontal plane. The polarimetric characteristics of the light source (corresponding to the parameters defined in Eqs. 3—6) are presented in Table 2.

Table 2. Polarimetric characteristics of the illumination used for performing the experiments.

Parameter	Mean value	Standard deviation
Azimuth angle	-0.64 (deg)	0.19
Ellipticity	-0.91 (deg)	0.29
Degree of polarization	99.93 (%)	0.29
Degree of linear polarization	99.88 (%)	0.27

2.1.3. Detection

As detector, a polarimetric camera of the model PHX050S-PC Lucid Vision Labs Phoenix was used with an objective model Edmund Optics 25 mm with the aperture set at f /1.4. It is a division of focal plane polarimetric camera of linear polarization. The sensor of this camera is based on micro-polarizer arrays. It has four linear polarizers (0 deg, 90 deg, 45 deg and 135 deg) grouped in one macro-pixel of 2x2 conventional pixels, i.e. each polarizer coincides with a pixel. A scheme of this configuration is shown in Fig. 3. Thus, it is able to recover the linear polarimetric information of light and permits to obtain the first three Stokes parameters: S_0, S_1 and S_2 for each macro-pixel in the image.

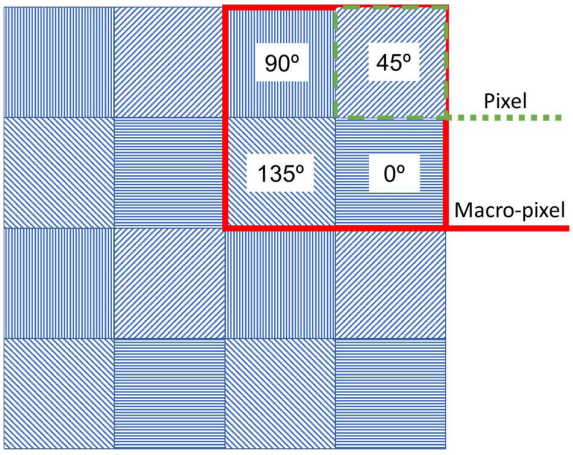

Figure 3. Scheme of the sensor of the polarimetric camera used as detector. In front of each pixel the corresponding polarizer is placed. The macro-pixel is the calculation unit.

2.1.4. Samples

To hold the samples of the different materials of study, a test plate organized in the form of a 2x2 matrix was used (see Fig. 4). From top left to bottom right of the test plate, in the position 1:1 there was a sample of a white sheet of paper; in 1:2 there was a sample of gray expanded polystyrene (EPS); in 2:1 a metallic object and in 2:2 a piece of wood. The edge of the plate was recovered with an optical absorbent duct tape which was considered the background. The amount of visible light reflected from the tape is negligible (below 5%).

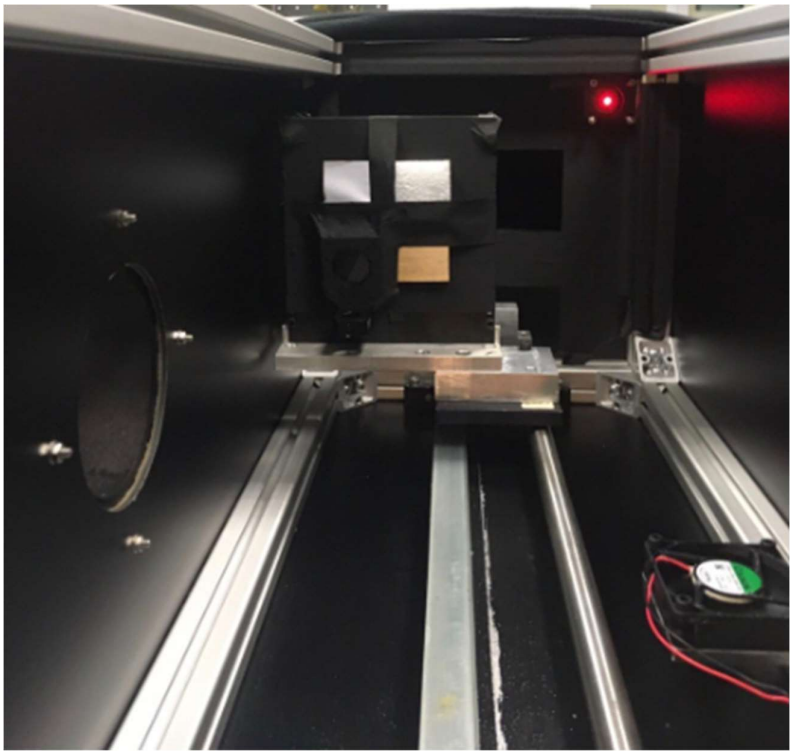

Figure 4. Test plate containing the targets of different materials inside the fog chamber.

The plate was placed inside the fog chamber in such a way that the polarimetric camera objective focused the image correctly on the sensor. To do this, the test plate was connected to a magnetic ruler built into the box, which allowed to move it on a cart and know precisely their position within the space.

The light intensity at the edges and the center of the plate was verified, in order to ensure that the illumination was evenly distributed. For that, intensity images of the setup without fog were taken. Grey levels were evaluated at different points of the images for different illumination configurations until all the plate was evenly illuminated. The final configuration showed a deviation in intensity between the edges and the center of the plate below 2%.

Prior to the experiments, a polarimetric characterization of the behavior of each of the elements of the test plate was carried out. Each of the samples was illuminated with the same linear polarization state that the one described in Table 2. The degree of linear polarization (DOLP) exhibited by the reflected illumination was evaluated. The results obtained are shown in Table 3. Paper, EPS and wood were depolarizing materials with similar characteristics, and they behaved differently from metal and the background. As expected, dielectric materials did not maintain polarization, while metal and, in this case, the small amount light reflected by background (Black Masking Tape) did.

Table 3. Degree of linear polarization of the reflected illumination for each of the elements of the test plate.

Material	DOLP
Paper	0.11
EPS	0.27
Metal	0.89
Wood	0.30
Background	0.75

2.2. Image processing

2.2.1. Imaging modes

Division of focal plane polarimetric cameras based on micro-polarizer arrays allow easy retrieval of images of the Stokes parameters [18]. As a result, in one shot, four images of the same scene corresponding to each of the polarization filters are obtained as raw images. With these data, the conventional intensity image can be calculated by simply adding two images with orthogonal polarizations. It is also possible to calculate the images corresponding to the linear Stokes parameters (S_1 and S_2), and other images based on usual parameters in polarimetry [15]. Table 4 shows all the image modes used in this study and also the acronym by which we will refer to them in the rest of this article. It is recalled that all those modes are simple linear combinations of the images obtained pixel by pixel or parameters usual in polarimetry. Our goal is now to compare the contrast obtained for each of these image modes through different fog transmittances.

Table 4. Imaging modes used in this study. From left to right: name, abbreviation taken in this article and means of obtaining them using the raw images (see Table 1).

Image mode name	Abbreviation	Computation
Intensity / Stokes 0	INT	$I_H + I_V = I_{45} + I_{135}$
Stokes 1	S_1	$I_H - I_V$
Stokes 2	S_2	$I_{45} - I_{135}$
Co-polarized	CO	I_H
Cross-polarized	$CROSS$	I_V
Degree of linear polarization	$DOLP$	$(S_1^2 + S_2^2)/INT$
Differential polarization	$DIFF$	$CO - CROSS$
Degree of co-polarization	POL	$DIFF/INT$

It should be noticed that the concept of co-polarization corresponds to the detection of polarized light in the same state as the polarization of the emitted light. Instead, the cross-polarization refers to the detection in the orthogonal state of that of the emission. In our case, the emission was at 0 deg, therefore CO is the image obtained through the 0 deg polarizer and CROSS the one corresponding to the 90 deg polarizer.

Fig. 5 shows an example of the recovered images at different fog transmittances for the different image modes proposed in Table 4.

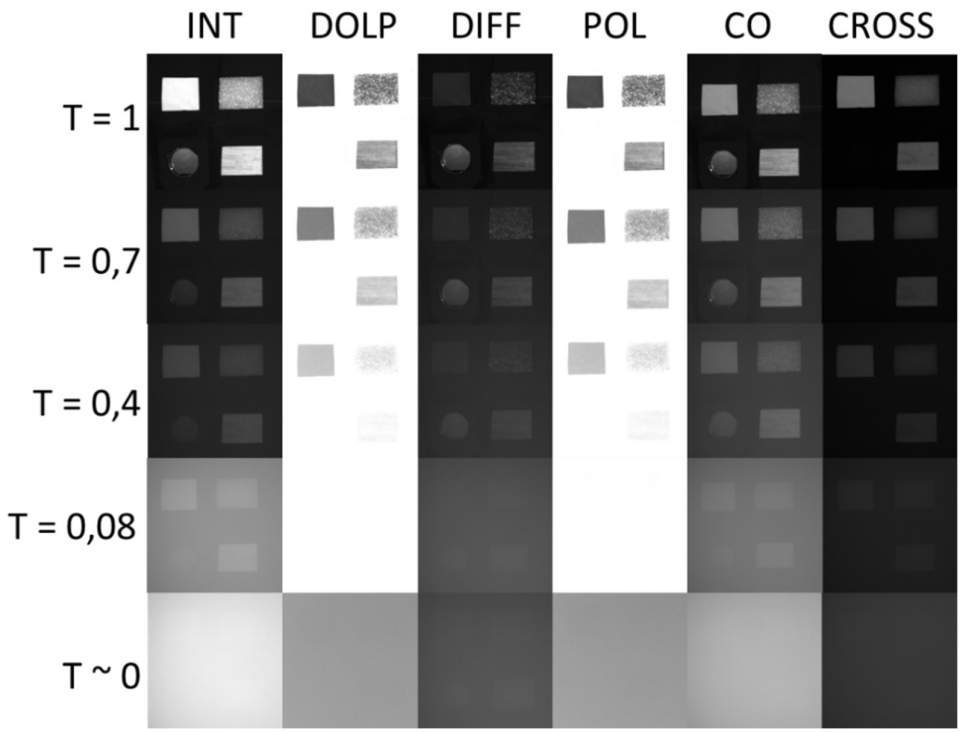

Figure 5. Images of the samples for the different image modes of Table 4 under different fog transmittances, arranged in rows. T = 1 (top) corresponds to absence of fog, while T ~ 0 (bottom) corresponds to the presence of very dense fog.

2.2.2. Michelson's contrast

Contrast is the difference in luminance that makes an object (or its representation in an image) distinguishable. In general, it is defined as the relative difference in intensity between two points in an image. It is usually used to quantify the ability to differentiate a sample from the background in which it is found. In the literature, there exist numerous ways of calculating the contrast in an image [19]. In this study, we have used Michelson's

contrast, as it is generally accepted as the most usual representation valid for all types of scenes when contrast is based on the most and the least intense points in the image irrespective of their surface area, frequency, or relative separation [20]. It is defined as:

$$C = |\frac{I_{obj} - I_{bg}}{I_{obj} + I_{bg}}|, \quad (8)$$

where I_{obj} is the average intensity of the sample of interest and I_{bg} is the average intensity of a zone of interest corresponding to the test plate covered with the absorbent Black Masking Tape.

3. Results

In order to define a standard visibility value, a contrast threshold of 0.05 (5%) is settled as the distinguishable limit for the human eye [21]. For the analysis of the results obtained, we will use this convention. Therefore, a sample with contrast below 5% will be considered as not detectable inside the fog.

Fig. 6 shows the evolution of the contrast between the selected sample and the background of the different image modes described in Table 4, for the four materials considered: a) paper, b) EPS, c) metal and d) wood, measured at 45 different fog transmittance levels. In each sub-figure the lower transmittance range has been expanded to better observe the behavior at the threshold of distinguishability. The results obtained for the dielectric materials (paper, wood and EPS) are comparable, while the metallic material behaves differently, in coherence with what was observed in Table 3.

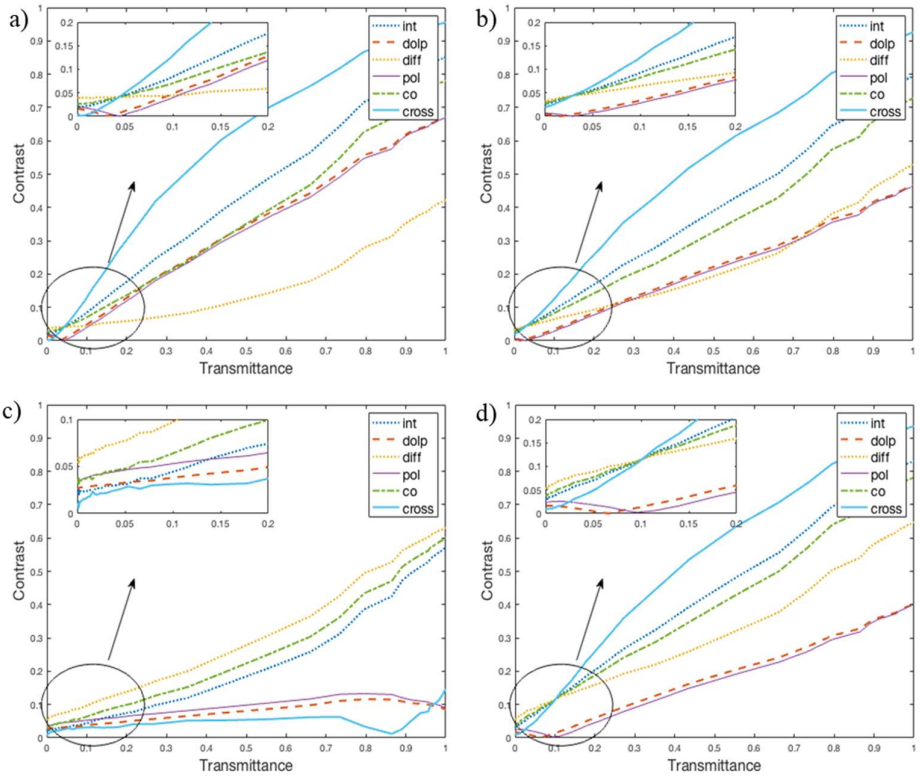

Figure 6. Michelson's contrast obtained for the image modes described in Table 4, at different transmittances. Each subfigure shows the result for a different material: (**a**) paper, (**b**) EPS, (**c**) metal; and (**d**) wood.

For very low transmittances (from T ~ 0 to T = 0.05), which correspond to very dense fog (expanded zones in Fig. 6), the contrast for the intensity mode is, in general, below the

visibility threshold (5%). Therefore, by using the intensity image it would not be possible to distinguish any of the samples through the fog. However, both the DIFF and CO polarimetric modes show higher contrasts. In the case of metal and wood, the DIFF mode exceeds the visibility threshold even for transmittances below 0.05, proving that polarimetric imaging modes can have advantages in detecting materials through foggy media. Thus, DIFF and CO modes enable to detect objects not distinguishable in the intensity image mode.

As a general trend, Fig.-6 shows there is always a polarimetric image mode that presents greater contrast than the intensity image, even for greater visibilities. In the case of dielectrics, the mode with the higher contrast corresponds to the CROSS image, while in the case of metal, the mode with the higher contrast is the DIFF image.

4. Discussion

The results presented in previous section show the advantages that the use of polarimetric imaging can bring in detection and segmentation of objects through turbid media. We proved that is possible to distinguish objects made with commonly encountered materials under the presence of fog, when conventional image fails. As it was mentioned in the introduction, this effect could have direct applications in fields related to transport in different media or surveillance in adverse weather conditions.

In general, backscattered light from targets exists primarily in the co-polarized component. For materials preserving polarization (such as metals), this effect is evident. In Fig. 5 it can be seen that metallic sample is not detectable in CROSS mode whereas it is in CO mode. Regarding dielectric materials, they are mainly depolarizing, so their images in CO mode are only slightly brighter than in CROSS mode. That can also be seen in Fig. 5. Finally, comparing CO and CROSS mode images in Fig. 5 for $T \sim 0$, we proved that the generated fog is mainly backscattering light in the co-polarized component, as long as the grey level in the CO mode is higher than in CROSS mode. In the end, contrast improvement is shown to be dependent upon the optical properties of the turbid media, the background and the target.

According to the results obtained for fog, the differential polarization image (DIFF) is the best mode for imaging through fog at very low visibilities for all the targets. In two of the four cases of study, the computed contrast is above the threshold of visibility for very small transmittances. DIFF mode, based on subtracting the cross-polarized component from the co-polarized one, is one of the most popular techniques for increasing contrast by means of polarization in biomedical microscopy [22]. This study shows that the same improvements presented through biological tissue can be obtained in fog. Moreover, we proved that this behavior is maintained for metallic targets even when visibility is increased.

Above the smallest transmittance values of fog, the CROSS mode presents to be outstanding for all dielectric samples. Fog reflects mainly co-polarized light, so the CROSS mode can be used to filter out its effect, or at least to mitigate it. As a result of the samples being depolarizing, co-polarized and cross-polarized components of reflected light from target are almost evened. That is why, once the amount of transmitted light returning for the objects is big enough, CROSS mode presents the highest contrast: it is used to clear the foggy effect of the image due to backscattered light. In the case of metal, only the co-polarized component of light is returning from the target and the small amount of light reflected by background is mostly co-polarized too, so the CROSS mode is not useful for metals under these conditions.

5. Conclusions

Michelson's contrast has been used as a metric to perform a study of contrast in foggy media on different materials, comparing a number of polarimetric imaging modes and the conventional intensity image. Following the conventional approach, we assumed that contrasts below 5% do not allow the eye to distinguish the sample of interest.

This study proves the usefulness of polarimetric imaging in turbid media, as it provides an interesting alternative to intensity images. For small transmittance (or low visibility), some of the polarimetric imaging modes have shown contrasts above the threshold of distinguishability, while the intensity mode stays always below it. This higher contrast has the potential to enable the detection and segmentation of objects in turbid media with greatly reduced visibility.

The different behavior between the studied materials has also been evaluated. In all cases and regardless of the type of material, for very small transmittances the mode with the highest contrast was the differential polarization image (DIFF). At the moment in which the transmittance increases, for materials with dielectric characteristics (wood, paper and expanded polystyrene), the image that presents the best contrast is that of cross-polarization (CROSS); while metal maintains the initial behavior, with DIFF always being the mode with better performance.

Author Contributions: Conceptualization, M.B., S.P. and S.R.; methodology, M.B. and S.P; software, A.V.; validation, M.B.; formal analysis, M.B. and A.V.; data curation, M.B.; writing—original draft preparation, M.B.; writing—review and editing, S.R.; supervision, S.R.; project administration, S.R.; All authors have read and agreed to the published version of the manuscript.

Funding: This research was funded by MINECO project FIS2017-89850-R, and by AGAUR Grants 020FI_B1 00185 and 2020FI_B2 00068, supported by the Secretaria d'Universitats i Recerca de la Generalitat de Catalunya and the Fons Social Europeu (FSE),

Conflicts of Interest: The authors declare no conflict of interest.

References

1. Xu, M.; Alfano, R.R. Random walk of polarized light in turbid media. *Phys. Rev. Lett.* **2005**, *95(21)*, pp. 213901. DOI: 10.1103/PhysRevLett.95.213901
2. Mackintosh, F. C.; et al. Polarization memory of multiply scattered light. *Phys. Rev. B.* **1989**, *40(13)*, pp. 9342. DOI: 10.1103/PhysRevB.40.9342
3. van der Laan, J. D.; Wright, J. B.; Scrymgeour, D. A.; Kemme, S. A.; Dereniak, E. L. Evolution of circular and linear polarization in scattering environments. *Opt. Express*, **2015**, *23(25)*, pp. 31874-31888. DOI: 10.1364/OE.23.031874
4. Lewis, G. D.; Jordan, D. L.; Roberts, P. J. Backscattering target detection in a turbid medium by polarization discrimination. *Appl. Opt.*, **1999**, *38(18)*, pp. 3937-3944. DOI: 10.1364/AO.38.003937
5. Kartazayeva, S. A.; Ni, X.; Alfano, R. R. Backscattering target detection in a turbid medium by use of circularly and linearly polarized light. *Opt. Lett.*, **2005**, *30(10)*, pp. 1168-1170. DOI: 10.1364/OL.30.001168
6. Walker, J. G.; Chang, P. C.; Hopcraft, K. I. Visibility depth improvement in active polarization imaging in scattering media. *Appl. Opt.*, **2000**, *39(27)*, pp. 4933-4941. DOI: 10.1364/AO.39.004933
7. Goudail, F.; Tyo, J.S. When is polarimetric imaging preferable to intensity imaging for target detection? *JOSA A.* **2011**, *Volume 28.1*, pp. 46-53. DOI: 10.1364/JOSAA.28.000046
8. Rozé, C.; Maheu, B.; Gréhan, G.; Menard, J. Evaluations of the sighting distance in a foggy atmosphere by Monte Carlo simulation. *Atmospheric Environment*, **1994**, *28(5)*, 769-775. DOI: 10.1016/1352-2310(94)90235-6
9. Judd, K. M.; Thornton, M. P.; Richards, A. A. Automotive sensing: assessing the impact of fog on LWIR, MWIR, SWIR, visible, and lidar performance. In Infrared Technology and Applications XLV (Vol. 11002, p. 110021F) SPIE; 2019. DOI: 10.1117/12.2519423
10. Schechner, Y. Y.; Narasimhan, S. G.; Nayar, S. K. Polarization-based vision through haze. *Appl. Opt.*, **2003**, *42(3)*, pp. 511-525. DOI: 10.1364/AO.42.000511
11. Rowe, M. P.; Pugh, E. N.; Tyo, J. S.; Engheta, N. Polarization-difference imaging: a biologically inspired technique for observation through scattering media. *Opt. Lett.*, **1995**, *20(6)*, pp. 608-610. DOI: 10.1364/OL.20.000608
12. Fade, J.; et al. Long-range polarimetric imaging through fog. *Appl. Opt.*, **2014**, *53(18)*, pp. 3854-3865. DOI: 10.1364/AO.53.003854
13. Tremblay, G.; Roy, G. Study of polarization memory's impact on detection range in natural water fogs. *Appl. Opt.*, **2020**, *59(7)*, pp. 1885-1895. DOI: 10.1364/AO.383480
14. Chipman, R. A. Polarimetry. In *Handbook of Optics*; Van Stryland, E. W.; Williams, D. R.; Wolfe, W. L. Eds; McGraw-Hill: New York, USA, 1995; Volume 2, pp. 22.1-22.37.
15. Nothdurft, R. E.; Yao, G. Effects of turbid media optical properties on object visibility in subsurface polarization imaging. *Appl. Opt.*, **2006,** *45(22)*, pp. 5532-5541. DOI: 10.1364/AO.45.005532

16. Novikova, T., Bénière, A., Goudail, F., De Martino, A. Contrast evaluation of the polarimetric images of different targets in turbid medium: possible sources of systematic errors. In Polarization: Measurement, Analysis, and Remote Sensing IX (Vol. 7672, p. 76720Q) SPIE; 2010. DOI: 10.1117/12.849907
17. Vannier, N., et al. Comparison of different active polarimetric imaging modes for target detection in outdoor environment. *Appl. Opt.*, **2016**, *55(11),* pp. 2881-2891. DOI: 10.1364/AO.55.002881
18. Hickman, D. L. Polarimetric imaging: system architectures and trade-offs. In Electro-Optical and Infrared Systems: Technology and Applications XV SPIE; 2018. DOI: 10.1117/12.2325320
19. Peli, E. Contrast in complex images. *JOSA A*, **1990**, *7(10),* pp. 2032-2040. DOI: 10.1364/JOSAA.7.002032
20. Bex, P. J.; Makous, W. Spatial frequency, phase, and the contrast of natural images. *JOSA A*, **2002**, *19(6),* pp. 1096-1106. DOI: 10.1364/JOSAA.19.001096
21. Dumont, E; Cavallo V. Extended Photometric Model of Fog Effects on Road Vision. *Transportation Research Record*, **2004**, *1862(1),* pp. 77-81. DOI: 10.3141/1862-09
22. Kim, M. et al. Differential polarization imaging. I. Theory. *Biophys. J.*, **1987**, *52(6),* pp. 911-927. DOI: 10.1016/S0006-3495(87)83285-X